Nanometer-Scale Infrared Spectroscopy of Heterogeneous Polymer Nanostructures Fabricated by Tip-Based Nanofabrication

Jonathan R. Felts,[†] Kevin Kjoller,[‡] Michael Lo,[‡] Craig B. Prater,[‡] and William P. King[†,*]

[†]Department of Mechanical Science and Engineering, University of Illinois Urbana—Champaign, Urbana, Illinois 61820, United States and [‡]Anasys Instruments, Santa Barbara, California 93101, United States

ABSTRACT

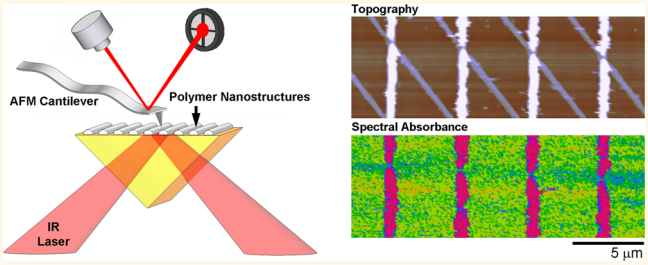

There is a significant need for chemical identification and chemical imaging of nanofabricated structures and devices, especially for multiple materials integrated at the nanometer scale. Here we present nanofabrication, chemical identification, and nanometer-scale chemical imaging of polymer nanostructures with better than 100 nm spatial resolution. Polymer nanostructures of polyethylene, polystyrene, and poly(3-dodecylthiophene-2,5-diyl) were fabricated by tip-based nanofabrication. Nanometer-scale infrared measurements using atomic force microscopy infrared spectroscopy (AFM-IR) obtained quantitative chemical spectra of these nanostructures. We show chemical imaging of intersecting patterns of nanometer-scale polymer lines of different chemical compositions. The results indicate that for closely packed heterogeneous nanostructures, the spatial resolution of AFM-IR is not limited by nanometer-scale thermal diffusion, but is instead limited by the cantilever sensitivity and the signal-to-noise ratio of the AFM-IR system.

KEYWORDS: atomic force microscope · AFM · thermal dip-pen nanolithography · tDPN · AFM-IR · photothermal induced resonance · nanolithography · tip based nanofabrication · TBN

Nanometer-scale chemical lithography technologies including nanoprinting,[1−4] and tip-based nanofabrication[5−8] are growing in complexity and capability, and can rapidly fabricate chemical patterns with sizes as small as 10 nm.[9] Using these nanofabrication technologies, it is possible to integrate and overlay patterns of different materials at the nanometer-scale. Here we refer to these nanometer-scale patterns of multiple discretely formed materials as heterogeneous chemical nanostructures. Despite the rapid advances in the fabrication of nanometer-scale chemical patterns, there has been much less research on chemical imaging and identification of nanometer-scale chemical patterns. There is a need for metrology that can identify the chemical structure and spatial extent of chemical nanopatterns.

In tip-based nanomanufacturing (TBN), a nanometer-scale tip or arrays of nanometer-scale tips can directly fabricate nanostructures by depositing,[5,10] removing,[11,12] or reacting[13,14] chemical species near the tip. Arrays of atomic force microscope (AFM)[15] tips can pattern heterogeneous chemical nanostructures by transferring molecules from tip to substrate with high throughput and nanometer-scale precision.[16,17] Heated AFM tips use temperature-induced chemical[14] or physical[10] transitions to pattern heterogeneous chemical nanostructures with useful electrical,[18] optical,[19] and biological[20] properties. Most research on tip-based nanomanufacturing has focused on fabrication and the performance of tip-written nanostructures, while few published articles focus on chemical analysis of the tip-written nanostructures. The challenge in identifying and diagnosing these chemical nanostructures is even more difficult when there are multiple chemical compounds that have been integrated at the nanometer scale. A key advantage of tip-based nanomanufacturing is its ability to fabricate closely packed nanostructures of different materials at the nanometer scale. Thus the lack of nanometer-scale chemical identification and imaging techniques limits the development of tip-based nanomanufacturing techniques and applications.

* Address correspondence to wpk@illinois.edu.

Received for review June 13, 2012 and accepted August 28, 2012.

Published online August 28, 2012
10.1021/nn302620f

In AFM-based infrared spectroscopy (AFM-IR), a rapidly pulsed IR laser is incident upon a thin sample, which absorbs the IR light and undergoes rapid thermomechanical expansion. An AFM tip in contact with the sample monitors the thermomechanical expansion. The AFM-IR system varies the wavelength of incident IR radiation and scans the tip over the sample surface. Thus the sample IR absorptivity can be measured as a function of wavelength and position, resulting in both structural and chemical information about the sample.[21−23] AFM-IR has been used to measure IR chemical absorption spectra on diverse materials such as biological cells,[24,25] organic thin films,[26] and semiconductor structures.[27−29] Several published articles explore the spatial resolution limits of AFM-IR.[23−29] The smallest achievable spatial resolution of AFM-IR is governed by the tip sharpness, as well as nanometer-scale IR absorption and thermal diffusion in the sample. The spatial resolution is also affected by nanometer-scale variations in the sample thermal diffusivity or IR absorptivity, which can complicate analysis of the measured photothermal expansion. It is such variations in structure and composition, however, which are typical in tip-fabricated nanostructures.

A few published articles investigate how nanometer-scale heat diffusion affects the spatial resolution of AFM-IR.[25,28,30] The simplest analysis is for the case of a sample that has homogeneous IR absorptivity, since the heat is uniformly generated within the sample and uniformly flows into the substrate. Thus, IR absorption contrast between the absorbing sample and the substrate determines spatial resolution. For example, AFM-IR of micrometer-sized bacteria on a nonabsorbing substrate had a spatial resolution of 100 nm.[25,30] Also for example, AFM-IR measurements on silicon oxide disks fabricated onto a silicon substrate had a spatial resolution of 50 nm.[28] While the spatial resolution of AFM-IR is reasonably good for nearly homogeneous samples, the spatial resolution is much poorer when the sample consists of multiple materials having spatially varying IR absorptivity. In this case, heat generated from IR absorption in one material flows into the nearby nonabsorbing material, and the resulting thermomechanical expansion of the nonabsorbing region cannot be easily decoupled from the thermomechanical expansion of the absorbing region. For example, AFM-IR on nonabsorbing bacteria that contained sparsely distributed absorbing virus particles of size 90 nm identified the virus particles as having an apparent size of 200 nm, due to thermal diffusion from the viruses to the surrounding bacteria.[24] Similarly, AFM-IR measurements of 20 nm quantum dots buried in silicon could identify the location of the quantum dot with a resolution of 60 nm.[27,29] Such local heat flow effects reduce the ability of AFM-IR to generate quantitative chemical spectra for materials identification. For example, AFM-IR on a polymer multilayer film stack cross section

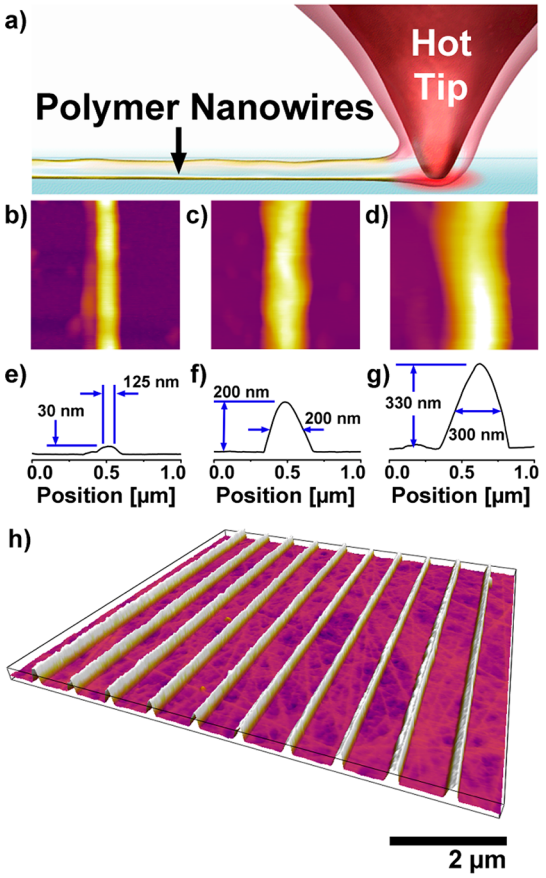

Figure 1. (a) Graphic representation of heated tip polymer deposition; (b−d) 1 μm square topography scans of written polymer nanowires and (e−g) accompanying topography profiles of nanowires 125−300 nm wide and 30−330 nm tall; (h) AFM topography image of a polymer nanowire array with lines spaced 1 μm apart.

could achieve good chemical spectra within 100 to 1000 nm of the polymer interfaces, even though the sample was very thin and the alternating polymer regions were 5−15 μm wide.[26,31] Overall, we can summarize the previous work on AFM-IR as follows: AFM-IR has been primarily used to study small regions of bulk samples, for which sample heterogeneity affects the spatial resolution due to nonuniform IR absorption and nanometer-scale heat flows. There is a lack of research on AFM-IR of nanofabricated structures, and the limits of doing so have not been investigated.

Here we present AFM-IR characterization of various polymer nanostructures and heterogeneous patterns of polymer nanostructures, where the structures and the resolution of the chemical characterization are both on the order of 100 nm. Polymer nanostructures of polyethylene (PE), polystyrene (PS), and poly(3-dodecylthiophene-2,5-diyl) (PDDT) were fabricated by tip-based nanofabrication. AFM-IR obtained chemical spectra of the fabricated nanostructures. We demonstrate chemical imaging at the interface between overlapping PE and PS nanostructures with a resolution of

100 nm, and a heat transfer analysis at the interface of the two structures shows that spatial resolution is not heat diffusion limited.

RESULTS AND DISCUSSION

We used a heated AFM tip to fabricate nanostructures of various polymers. Heated tips can control deposition of thermoplastic polymers,[10,19,20,32−34] low temperature metals,[35] thiols,[36] and polymer−nanoparticle composites.[8] Figure 1a shows a schematic of a heated tip depositing a polymer nanowire, where a molten polymer ink flows from the tip to the surface when the tip is hot. When the tip is cold, no polymer flows, such that temperature can control the nanostructure fabrication.[8,10] The tip has an integrated solid state heater that can control the temperature, and a wear-resistant diamond coating that enhances ink wettability.[37,38] The tip speed and tip temperature affect the size and shape of the deposited polymer. Figure 1 panels b−h show polyethylene features with widths between 125 and 300 nm and heights between 30 and 330 nm, and a uniform spacing of 1 μm. We fabricated nanostructures of polyethylene (PE), polystyrene (PS), and poly(3-dodecylthiophene-2, 5-diyl) (PDDT) with feature sizes ranging between 100 and 1000 nm. The polymer nanostructures were written in close proximity on the same substrate, with some nanostructures overlapping.

We measured the chemical composition and spatial extent of the polymer nanostructures using an AFM-IR system based on photothermal detection. Figure 2a shows AFM-IR, where a tunable IR laser illuminates the polymer nanostructures to induce rapid thermomechanical expansion. An AFM tip in contact with the polymer nanostructure resonates in response to the expansion, and this resonance is measured by the AFM. Figure 2b,c show the time-domain and frequency-domain cantilever responses for PE nanostructures irradiated at 2920 cm^{-1} after applying a frequency bandpass filter between 200 and 260 kHz. The peak-to-peak amplitude of the time data provides a measure of IR absorption, and the location of the peaks in the frequency domain provide a qualitative measure of local material stiffness. The cantilever amplitude is sensitive to the expansion rate of the nanostructure, which allows AFM-IR to measure substrate expansion below 1 nm.[39] Figure 2b,c shows the measured AFM-IR signals for PE nanostructures for heights of 80, 400, or 1000 nm, indicating absorption can be measured at 2920 cm^{-1} for features down to 80 nm in height.

Measuring the cantilever response while sweeping the IR laser wavelength produces absorption spectra that compare well to bulk spectra. We measured the IR absorption spectra of the polymer nanostructures by sweeping the wavenumber of the incident IR laser and measuring the cantilever response at each wavenumber. Figure 3 shows the absorption spectra of the PE nanostructures for wavenumbers in the range

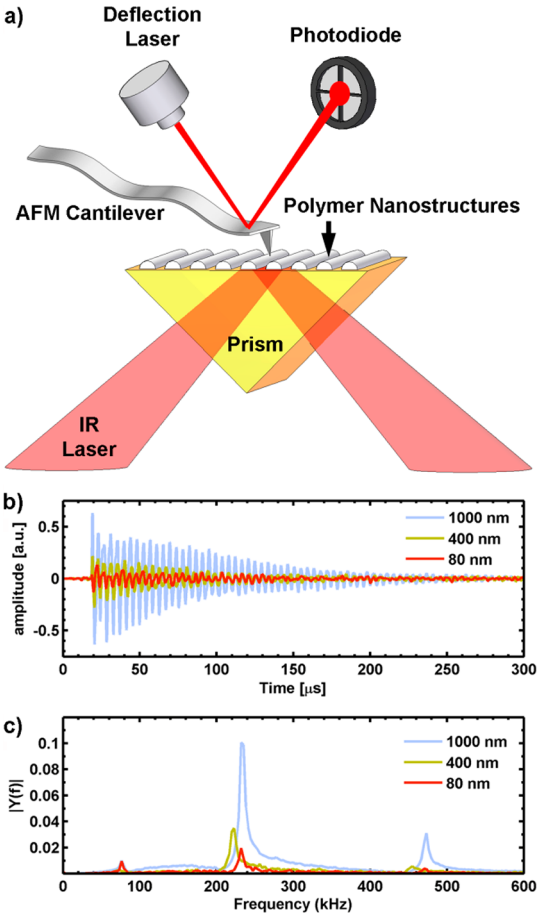

Figure 2. (a) Graphical representation of polymer nanowire AFM-IR measurements; (b) oscillatory AFM cantilever response to rapid expansion of polyethylene nanowires with heights between 80 and 1000 nm; (c) frequency response of the AFM cantilever computed with fast Fourier transforms.

1250−1550 cm^{-1} and 2800−3100 cm^{-1}. The peak near 2926 cm^{-1} corresponds to the antisymmetric C−H stretch of the PE hydrocarbon backbone, and the 2860 cm^{-1} peak arises from the hydrocarbon symmetric C−H stretch. A small red-shift for the 1000 nm PE wire indicates a lower chain order compared to the smaller wires. A hydrocarbon C−H scissoring peak appears near 1470 cm^{-1}. The polymer nanostructure thermal expansion depends on feature size, so the cantilever response amplitude decreases as the polymer feature size decreases. The cantilever amplitude from the C−H stretch absorption peaks was resolved for PE features as small as 80 nm tall, and cantilever amplitude from the C−H scissoring peak was resolved for features down to 400 nm. Thus, AFM-IR can determine chemical composition and local polymer order by measuring IR absorption spectra of polymer nanostructures smaller than 100 nm.

AFM-IR can generate unique IR spectra for many different polymer nanostructures, which can be used to identify nanostructure composition. Although AFM-IR cannot measure absolute sample absorptivity, the relative absorptivity spectra generated by AFM-IR

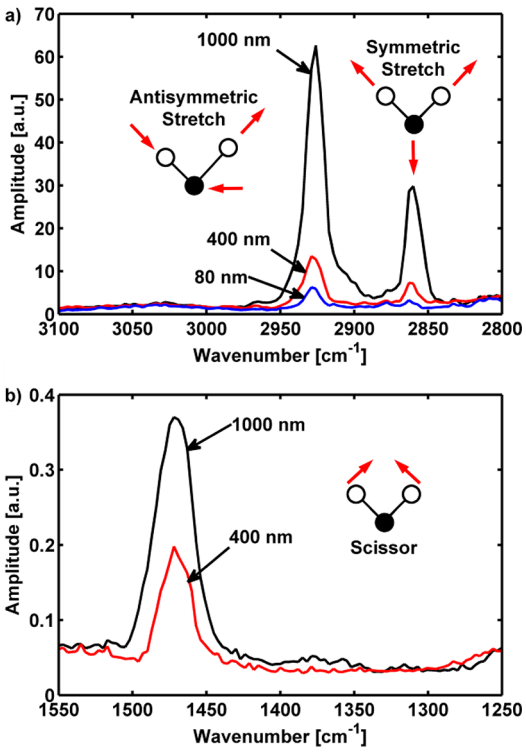

Figure 3. (a) Polyethylene absorption spectra for wavenumbers between 2800 and 3100 cm^{-1} for nanowires with heights between 80 and 1000 nm, which shows C−H symmetric stretch at 2860 cm^{-1} and antisymmetric stretch near 2926 cm^{-1} for all wire heights. (b) The absorption spectrum for wavenumbers between 1250 and 1550 cm^{-1}, showing the C−H scissoring vibration for the 400 and 1000 nm tall wires at 1470 cm^{-1}.

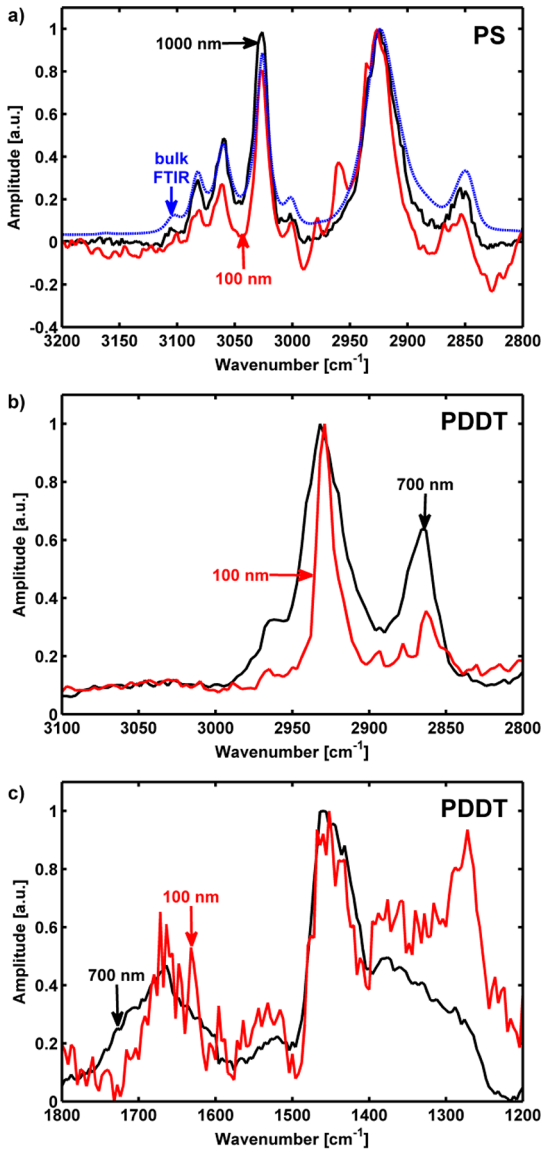

Figure 4. (a) Absorption spectra for 100 nm (red) and 1000 nm (black) tall polystyrene nanowires between 2800 and 3200 cm^{-1}, with a bulk FTIR spectra (blue) for comparison. There are two C−H stretch peaks near 2860 cm^{-1} and 2926 cm^{-1} from the hydrocarbon backbone, and additional peaks between 3000 and 3100 cm^{-1} corresponding to benzene ring C−H stretching. (b) Absorption spectra for 100 and 700 nm tall PDDT wires between 2800 and 3100 cm^{-1}, showing C−H stretch peaks near 2860 cm^{-1} and 2930 cm^{-1}. (c) Absorption of 100 and 700 nm tall PDDT wires between 1200 and 1800 cm^{-1}, showing broad absorption bands due to conjugated thiophene rings.

provides absorption peak locations and peak ratios sufficient to identify many different chemistries.[26] Figure 4 shows the IR absorption spectra for PS and PDDT nanostructures with heights between 100 and 1000 nm. The PS nanostructures have C−H stretch peaks near 2854 cm^{-1} and 2926 cm^{-1} from the hydrocarbon backbone. Three additional peaks arise from benzene ring C−H stretch between 3000 and 3100 cm^{-1}. For the 100 nm tall structure, there are additional peaks between 2950 and 3000 cm^{-1}, which we believe are noise and artifacts due to laser power drift relative to the measured background. Figure 4 panels b and c shows the absorption spectra of 100 and 700 nm tall PDDT nanostructures. The hydrocarbon backbone absorbs near 2864 and 2932 cm^{-1}, with a small shoulder peak near 2960 cm^{-1}. The thiophene ring of the PDDT has broad absorption bands in the range 1200−1800 cm^{-1}. For the 100 nm tall structure, low signal-to-noise affects the peak intensities of the measured signal. Despite the low signal-to-noise on the 100 nm tall structures, we can still distinguish between nanostructures of PE, PS, and PDDT. Overall, AFM-IR can identify the chemical composition of PS and PDDT polymer nanostructures as small as 100 nm.

Future device development requires measurement of the spatial organization of multiple interacting nanostructures. We use AFM-IR to identify the chemical composition of multiple overlapping polymer nanostructures. Lines of PS were drawn with a height of 600 nm and a 5 μm pitch, followed by 100 nm tall lines overlapping the PS structures at a 45° angle. Figure 5a shows an AFM topography map of the written nanostructure pattern. While the pattern was irradiated at a single wavenumber, a cantilever scanned over the pattern and measured absorption at each scan point. Figure 5b shows the spatial absorption map for

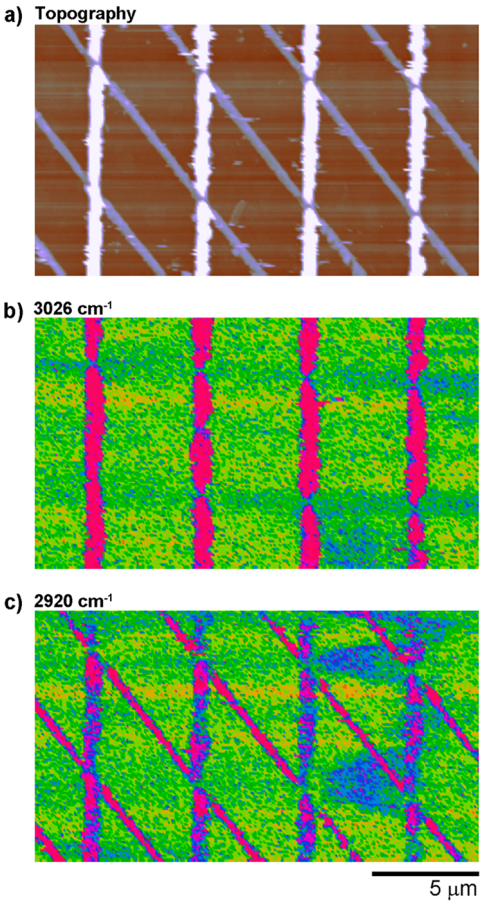

Figure 5. (a) AFM topography image of overlapping 600 nm tall PS nanowires (vertical features) and 100 nm tall PE nanowires (angled features). (b) Single wavenumber absorption image of the overlapping nanowires at 3026 cm^{-1}, showing only the PS nanowire absorption. (c) Absorption image at 2920 cm^{-1}, revealing absorption of both PS and PE wires.

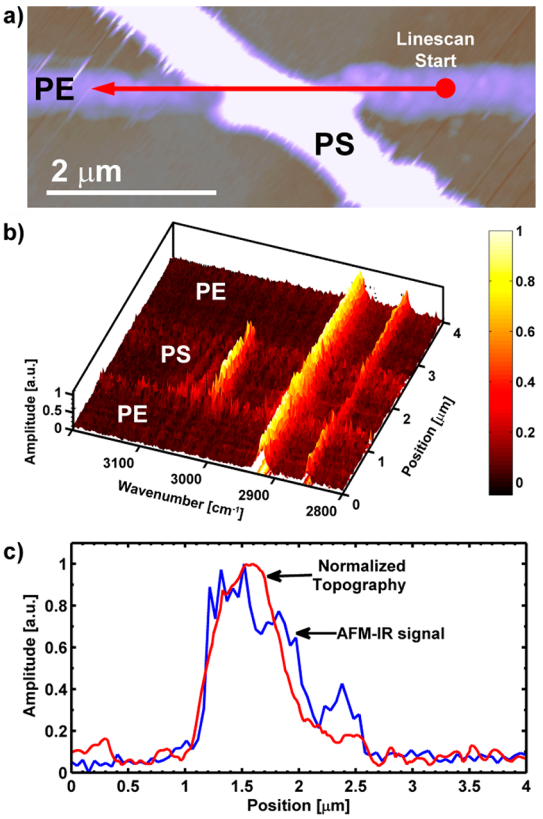

Figure 6. (a) AFM topography scan of 600 nm tall PS and 100 nm tall PE nanowire intersection. Absorption spectra were measured every 50 nm for the 4 μm line scan trajectory shown (red arrow). (b) Normalized absorption spectra measured during the line scan as a function of both wavenumber and position. (c) The absorption amplitude at 3025 cm^{-1} wavenumber as a function of tip scan position, showing a resolution which matches the PS line topography.

wavenumber 3026 cm^{-1}, corresponding to the largest C−H stretch of the PS benzene ring. The absorption map shows absorption only in the PS structures. Figure 5c shows the spatial absorption map for wavenumber 2920 cm^{-1} corresponding to a common absorption peak for the two polymers, and the cantilever detected absorption in both materials. These results demonstrate chemical identification of fabricated nanostructure architectures over a large scan area.

Many organic materials have similar absorption peaks and require information from broad absorption spectra to distinguish between them. Figure 6a shows an AFM topography image of the interface between overlapping PS and PE nanostructures. Absorption spectra were measured between 2800 and 3200 cm^{-1} with 50 nm separation in a linescan over the interface. Figure 6b shows normalized absorption plotted against both position and wavenumber. As expected, the PE nanostructure only absorbed near 2860 cm^{-1} and 2930 cm^{-1}, while the PS structure showed additional peaks between 3000 and 3100 cm^{-1}. Figure 6c shows single wavenumber absorption at 3026 cm^{-1} for each location along the linescan. The absorption amplitude is proportional to the topography of the PS nanostructure, and the absorption signal at the boundary between the PE and PS structures at 1.1 μm decreases to the background signal within 100 nm.

We consider whether the AFM-IR spatial resolution at the interface between the two polymer nanostructures is limited by heat diffusion or the radius of the AFM tip. To understand the effect of heat diffusion on spatial resolution at the interface between two nanostructures, we performed a 3D finite element transient heat transfer analysis. The model considered heat generation within the polymer, the transient temperature distribution in the polymer, and between adjacent polymer nanostructures, and heat flow into the substrate (see Supporting Information). The analysis revealed that at a distance of 100 nm away from the interface, the maximum temperature of the PE nanostructure reaches only 8% of the maximum temperature of the PS nanostructure. Since the nanostructure expansion is linearly proportional to temperature rise, the PE nanostructure undergoes negligible expansion within 100 nm of the PS interface. The temperature rise of the PE nanostructure 20 nm away from the PS-PE interface is only 33% of the PS structure maximum

temperature. This is a significant temperature drop within a distance of about one AFM tip radius. Thus for AFM-IR near this interface, the lateral spatial resolution is limited by the size and shape of the AFM tip and not heat diffusion. The large temperature drop in the vicinity of the interface arises because 90% of the heat generated within the PS nanostructure flows to the ZnSe prism. Because the majority of the heat generated within the PS nanostructure flows to the substrate, thermal diffusion does not induce a significant temperature rise in the nonabsorbing PE nanostructure, and so does not cause a significant thermomechanical expansion. Since thermal diffusion is not responsible for the absorption amplitude decrease at the interfaces in Figure 6c, the topography of the PS nanostructure governs the observed decrease. We resolve the topography-dependent absorption amplitude with a 50 nm resolution equal to the distance between data points, such that that the tip radius and the measurement lateral spacing determine the overall spatial resolution of AFM-IR absorption measurements presented here. Overall we conclude that for the heterogeneous chemical nanostructures of the present study, the lateral spatial resolution of AFM-IR is limited by the AFM tip radius, and not by thermomechanical expansion. Additionally, the cantilever sensitivity and the AFM-IR system signal-to-noise characteristics must be sufficient to detect the nanostructure expansion.

Chemical identification at the nanometer-scale is critical for the future development of nanomanufacturing, since it will be essential to perform chemical as well as structural metrology on future nanometer-scale devices. Here we have demonstrated that AFM-IR is capable of such imaging and chemical identification of nanofabricated polymer nanostructures, with a spatial resolution of 100 nm. This is in contrast to previous publications that focused on nanometer-scale characterization of bulk materials, for which the spatial resolution was limited by nanometer-scale heat flow within the sample. For the polymer nanostructures studied here, the spatial resolution of AFM-IR is not limited by nanometer-scale heat flow but rather the signal-to-noise ratio of the AFM-IR system and the cantilever sensitivity. We suggest that work could focus on further improving the signal-to-noise ratio of the AFM-IR system.

CONCLUSION

AFM-IR enables nanometer-scale IR spectroscopy of heterogeneous chemical nanostructures patterned by means of tip-based nanofabrication. The technique was demonstrated by measuring the IR absorption of PE, PS, and PDDT nanostructures with heights as small as 80 nm. Absorption maps generated for overlapping PS and PE nanostructures showed a spatial resolution on the order of 100 nm. We investigated the effect of thermal diffusion at the boundary between two nanostructures with a finite element analysis and found that thermal diffusion does not limit spatial resolution. Interrogating local chemical composition of heterogeneous chemical nanostructures will prove increasingly useful as the complexity of both the lithographic process and the desired pattern increases.

METHODS

Coating the Heated AFM Tip with Polymer. The tip was coated with PS and PDDT by dipping the heated tip into toluene containing either PS or PDDT. The polymer remained on the tip after the toluene evaporated. To coat the heated tip with PE, a polymer that is not soluble in most solvents, the tip was heated to 150 °C and inserted into a solid PE pellet. In both coating methods, heating the tip while scanning in contact on a substrate removed extra polymer and left a thin layer of polymer to be used for fabricating polymer nanostructures.

Heterogeneous Chemical Nanostructure Fabrication. Nanostructures were fabricated using a heated AFM tip with an Asylum MFP-3D AFM. The coated tips deposited structures onto a zinc selenide prism by scanning in contact with the prism while heated above the glass transition temperature of the polymer coating surrounding the tip. An electronic feedback loop held a constant temperature at the AFM tip heater by maintaining a constant heater electrical resistance. Tip speeds between 0.1 and 2 μm/s and temperatures between 120 and 300 °C determined the size of the patterned nanostructures.

Atomic Force Microscope Infrared Spectroscopy. Infrared spectroscopy of patterned nanostructures was performed with an Anasys Instruments nanoIR AFM. An Ekspla optical parametric oscillator laser irradiated the nanostructures with IR light between 2.5 and 10 μm wavelength. Spectra of nanostructures were generated by measuring the thermomechanical expansion of each structure as a function of irradiation wavelength and dividing by the measured laser spectral intensity.

Conflict of Interest: The authors declare the following competing financial interest(s): The authors have financial interest in Anasys Instruments, which sells infrared and AFM instrumentation.

Acknowledgment. We are grateful for support from AFOSR MURI FA9550-08-1-0407, and the DARPA TBN program. This research is supported in part by the Department of Energy Office of Science Graduate Fellowship Program (DOE SCGF), made possible in part by the American Recovery and Reinvestment Act of 2009, administered by ORISE-ORAU under contract no. DE-AC05-06OR23100.

Supporting Information Available: A 3D finite element model of transient heat transfer at the boundary between two polymer nanostructures. This material is available free of charge *via* the Internet at http://pubs.acs.org.

REFERENCES AND NOTES

1. Xia, Y. N.; Whitesides, G. M. Soft Lithography. *Annu. Rev. Mater. Sci.* **1998**, *28*, 153–184.
2. Chou, S. Y.; Krauss, P. R.; Renstrom, P. J. Imprint of Sub-25 Nm Vias and Trenches in Polymers. *Appl. Phys. Lett.* **1995**, *67*, 3114–3116.
3. Bailey, T.; Choi, B. J.; Colburn, M.; Meissl, M.; Shaya, S.; Ekerdt, J. G.; Sreenivasan, S. V.; Willson, C. G. Step and Flash Imprint Lithography: Template Surface Treatment and Defect Analysis. *J. Vac. Sci. Technol. B* **2000**, *18*, 3572–3577.
4. Park, J. U.; Hardy, M.; Kang, S. J.; Barton, K.; Adair, K.; Mukhopadhyay, D. K.; Lee, C. Y.; Strano, M. S.; Alleyne,

A. G.; Georgiadis, J. G.; *et al.* High-Resolution Electrohydrodynamic Jet Printing. *Nat. Mater.* **2007**, *6*, 782–789.
5. Piner, R. D.; Zhu, J.; Xu, F.; Hong, S. H.; Mirkin, C. A. "Dip-Pen" Nanolithography. *Science* **1999**, *283*, 661–663.
6. Demers, L. M.; Ginger, D. S.; Park, S. J.; Li, Z.; Chung, S. W.; Mirkin, C. A. Direct Patterning of Modified Oligonucleotides on Metals and Insulators by Dip-Pen Nanolithography. *Science* **2002**, *296*, 1836–1838.
7. Huo, F. W.; Zheng, Z. J.; Zheng, G. F.; Giam, L. R.; Zhang, H.; Mirkin, C. A. Polymer Pen Lithography. *Science* **2008**, *321*, 1658–1660.
8. Lee, W. K.; Dai, Z. T.; King, W. P.; Sheehan, P. E. Maskless Nanoscale Writing of Nanoparticle-Polymer Composites and Nanoparticle Assemblies Using Thermal Nanoprobes. *Nano Lett.* **2010**, *10*, 129–133.
9. Austin, M. D.; Ge, H.; Wu, W.; Li, M.; Yu, Z.; Wasserman, D.; Lyon, S. A.; Chou, S. Y. Fabrication of 5 Nm Linewidth and 14 Nm Pitch Features by Nanoimprint Lithography. *Appl. Phys. Lett.* **2004**, *84*, 5299–5301.
10. Sheehan, P. E.; Whitman, L. J.; King, W. P.; Nelson, B. A. Nanoscale Deposition of Solid Inks *via* Thermal Dip Pen Nanolithography. *Appl. Phys. Lett.* **2004**, *85*, 1589–1591.
11. Xu, S.; Miller, S.; Laibinis, P. E.; Liu, G. Y. Fabrication of Nanometer Scale Patterns within Self-Assembled Monolayers by Nanografting. *Langmuir* **1999**, *15*, 7244–7251.
12. Pires, D.; Hedrick, J. L.; De Silva, A.; Frommer, J.; Gotsmann, B.; Wolf, H.; Despont, M.; Duerig, U.; Knoll, A. W. Nanoscale Three-Dimensional Patterning of Molecular Resists by Scanning Probes. *Science* **2010**, *328*, 732–735.
13. Muller, W. T.; Klein, D. L.; Lee, T.; Clarke, J.; McEuen, P. L.; Schultz, P. G. A Strategy for the Chemical Synthesis of Nanostructures. *Science* **1995**, *268*, 272–273.
14. Szoszkiewicz, R.; Okada, T.; Jones, S. C.; Li, T. D.; King, W. P.; Marder, S. R.; Riedo, E. High-Speed, Sub-15 Nm Feature Size Thermochemical Nanolithography. *Nano Lett.* **2007**, *7*, 1064–1069.
15. Binnig, G.; Quate, C. F.; Gerber, C. Atomic Force Microscope. *Phys. Rev. Lett.* **1986**, *56*, 930–933.
16. Hong, S.; Zhu, J.; Mirkin, C. A. Multiple Ink Nanolithography: Toward a Multiple-Pen Nano-Plotter. *Science* **1999**, *286*, 523–525.
17. Ming, Z.; David, B.; Sung-Wook, C.; Seunghun, H.; Kee, S. R.; Zhifang, F.; Chad, A. M.; Chang, L. A MEMS Nanoplotter with High-Density Parallel Dip-Pen Nanolithography Probe Arrays. *Nanotechnology* **2002**, *13*, 212.
18. Wei, Z. Q.; Wang, D. B.; Kim, S.; Kim, S. Y.; Hu, Y. K.; Yakes, M. K.; Laracuente, A. R.; Dai, Z. T.; Marder, S. R.; Berger, C.; *et al.* Nanoscale Tunable Reduction of Graphene Oxide for Graphene Electronics. *Science* **2010**, *328*, 1373–1376.
19. Fenwick, O.; Bozec, L.; Credgington, D.; Hammiche, A.; Lazzerini, G. M.; Silberberg, Y. R.; Cacialli, F. Thermochemical Nanopatterning of Organic Semiconductors. *Nat. Nanotechnol.* **2009**, *4*, 664–668.
20. Wang, D. B.; Kodali, V. K.; Underwood, W. D.; Jarvholm, J. E.; Okada, T.; Jones, S. C.; Rumi, M.; Dai, Z. T.; King, W. P.; Marder, S. R.; *et al.* Thermochernical Nanolithography of Multifunctional Nanotemplates for Assembling Nano-Objects. *Adv. Funct. Mater.* **2009**, *19*, 3696–3702.
21. Betzig, E.; Trautman, J. K. Near-Field Optics—Microscopy, Spectroscopy, and Surface Modification Beyond the Diffraction Limit. *Science* **1992**, *257*, 189–195.
22. Knoll, B.; Keilmann, F. Near-Field Probing of Vibrational Absorption for Chemical Microscopy. *Nature* **1999**, *399*, 134–137.
23. Dazzi, A.; Prazeres, R.; Glotin, E.; Ortega, J. M. Local Infrared Microspectroscopy with Subwavelength Spatial Resolution with an Atomic Force Microscope Tip Used as a Photothermal Sensor. *Opt. Lett.* **2005**, *30*, 2388–2390.
24. Dazzi, A.; Prazeres, R.; Glotin, F.; Ortega, J. M.; Al-Sawaftah, M.; de Frutos, M. Chemical Mapping of the Distribution of Viruses into Infected Bacteria with a Photothermal Method. *Ultramicroscopy* **2008**, *108*, 635–641.
25. Mayet, C.; Dazzi, A.; Prazeres, R.; Allot, E.; Glotin, E.; Ortega, J. M. Sub-100 Nm IR Spectromicroscopy of Living Cells. *Opt. Lett.* **2008**, *33*, 1611–1613.
26. Kjoller, K.; Felts, J. R.; Cook, D.; Prater, C. B.; King, W. P. High-Sensitivity Nanometer-Scale Infrared Spectroscopy Using a Contact Mode Microcantilever with an Internal Resonator Paddle. *Nanotechnology* **2010**, *21*, 185705.
27. Houel, J.; Sauvage, S.; Boucaud, P.; Dazzi, A.; Prazeres, R.; Glotin, F.; Ortega, J. M.; Miard, A.; Lemaitre, A. Ultraweak-Absorption Microscopy of a Single Semiconductor Quantum Dot in the Midinfrared Range. *Phys. Rev. Lett.* **2007**, *99*, 4.
28. Houel, J.; Homeyer, E.; Sauvage, S.; Boucaud, P.; Dazzi, A.; Prazeres, R.; Ortega, J. M. Midinfrared Absorption Measured at a Lambda/400 Resolution with an Atomic Force Microscope. *Opt. Express* **2009**, *17*, 10887–10894.
29. Sauvage, S.; Driss, A.; Réveret, F.; Boucaud, P.; Dazzi, A.; Prazeres, R.; Glotin, F.; Ortéga, J. M.; Miard, A.; Halioua, Y.; *et al.* Homogeneous Broadening of the S to P Transition in Ingaas/Gaas Quantum Dots Measured by Infrared Absorption Imaging with Nanoscale Resolution. *Phys. Rev. B* **2011**, *83*, 035302.
30. Dazzi, A.; Prazeres, R.; Glotin, F.; Ortega, J. M. Local Infrared Microspectroscopy with Subwavelength Spatial Resolution with an Atomic Force Microscope Tip Used as a Photothermal Sensor. *Opt. Lett.* **2005**, *30*, 2388–2390.
31. Van Eerdenbrugh, B.; Lo, M.; Kjoller, K.; Marcott, C.; Taylor, L. S. Nanoscale Mid-Infrared Evaluation of the Miscibility Behavior of Blends of Dextran or Maltodextrin with Poly(vinylpyrrolidone). *Mol. Pharm.* **2012**, *9*, 1459–1469.
32. Yang, M.; Sheehan, P. E.; King, W. P.; Whitman, L. J. Direct Writing of a Conducting Polymer with Molecular-Level Control of Physical Dimensions and Orientation. *J. Am. Chem. Soc.* **2006**, *128*, 6774–6775.
33. Laracuente, A. R.; Yang, M.; Lee, W. K.; Senapati, L.; Baldwin, J. W.; Sheehan, P. E.; King, W. P.; Erwin, S. C.; Whitman, L. J. Reversible Electron-Induced Conductance in Polymer Nanostructures. *J. Appl. Phys.* **2010**, *107*, 103723.
34. Lee, W. K.; Robinson, J. T.; Gunlycke, D.; Stine, R. R.; Tamanaha, C. R.; King, W. P.; Sheehan, P. E. Chemically Isolated Graphene Nanoribbons Reversibly Formed in Fluorographene Using Polymer Nanowire Masks. *Nano Lett.* **2011**, 5461–5464.
35. Nelson, B. A.; King, W. P.; Laracuente, A. R.; Sheehan, P. E.; Whitman, L. J. Direct Deposition of Continuous Metal Nanostructures by Thermal Dip-Pen Nanolithography. *Appl. Phys. Lett.* **2006**, *88*, 3.
36. Chung, S.; Felts, J. R.; Wang, D.; King, W. P.; De Yoreo, J. J. Temperature-Dependence of Ink Transport During Thermal Dip-Pen Nanolithography. *Appl. Phys. Lett.* **2011**, *99*, 193101.
37. Fletcher, P. C.; Felts, J. R.; Dai, Z. T.; Jacobs, T. D.; Zeng, H. J.; Lee, W.; Sheehan, P. E.; Carlisle, J. A.; Carpick, R. W.; King, W. P. Wear-Resistant Diamond Nanoprobe Tips with Integrated Silicon Heater for Tip-Based Nanomanufacturing. *ACS Nano* **2010**, *4*, 3338–3344.
38. Felts, J. R.; Somnath, S.; Ewoldt, R. H.; King, W. P. Nanometer-Scale Flow of Molten Polyethylene from a Heated Atomic Force Microscope Tip. *Nanotechnology* **2012**, *23*, 215301.
39. Dazzi, A.; Glotin, F.; Carminati, R. Theory of Infrared Nanospectroscopy by Photothermal Induced Resonance. *J. Appl. Phys.* **2010**, *107*, 124519–7.